Analysis of Soil Consolidation Behavior Using Pressuremeter Testing

Etude de la consolidation en utilisant le pressiomètre

Jacques Monnet[1#], *Luc* Boutonnier[2]

[1] *GAIATECH, 22 rue Antoine Chollier, 38170, Seyssinet, France**
[2] *EGIS Géotechnique, 3 Rue Docteur Schweitzer 38180 Seyssins, France*
[#]*Corresponding author: monnet.jacques@gaiatech.fr*

ABSTRACT

The pressuremeter test is typically interpreted using a linear elasto-plastic model, but soil permeability and saturation levels can complicate the interpretation, particularly regarding whether the modulus obtained is effective or apparent. Advancements in the ARSCOP project allow for calculating an effective modulus in nearly saturated fine soils, where the skeleton is linear and the pore fluid is a compressible water-air mixture. A non-linear elastic model has been developed, which accounts for modulus variation along radius around the probe. This model links pore pressure generation during the test to the soil's non-linear elasticity. In fine soils with compressible fluids, pore pressure dissipation follows a one-dimensional radial consolidation process, similar to one-dimensional vertical consolidation in oedometers. A new theoretical approach introduces the pressuremeter consolidation coefficient (c_h), which depends on the soil's elastic modulus and horizontal permeability, and has been validated through tests on Bransley clay.

RESUME

L'essai pressiométrique est habituellement interprété à l'aide d'un modèle élasto-plastique linéaire, mais cette approche peut être inexacte selon la perméabilité et le degré de saturation du sol, qui influencent la réponse drainée ou non drainée. Il devient alors difficile de distinguer entre un module effectif et apparent. Dans le cadre du projet ARSCOP, des progrès ont permis de calculer un module effectif pour les sols fins quasi saturés, en modélisant un fluide interstitiel compressible (mélange eau-air). Ce modèle permet également d'estimer la pression interstitielle générée lors de l'essai. Une nouvelle approche plus réaliste a été développée, prenant en compte le comportement élastique non linéaire du sol et la variation de la déformation autour de la sonde. Il a été démontré que la génération de pression interstitielle est liée à cette non-linéarité. Dans les sols fins à fluide compressible, la dissipation de la pression suit une consolidation unidimensionnelle radiale, similaire à celle verticale observée dans les œdomètres. Un coefficient de consolidation pressiométrique horizontal (c_h) a été introduit, validé par des tests sur l'argile de Bransley.

Keywords: pressuremeter; consolidation; Bransley clay.

1. Introduction

The pressuremeter test is often interpreted by considering the soil as linearly elasto-plastic. However, depending on the soil's permeability and its degree of saturation, the soil's response may be drained or undrained. Consequently, from a theoretical standpoint, it is sometimes difficult to determine whether the modulus measured during the pressuremeter test is an effective modulus or an apparent one. As part of the ARSCOP project, an initial milestone has been reached, enabling the calculation of the effective modulus for a nearly saturated fine soil, in which the skeleton exhibits a linear response and the pore fluid is a compressible water-air mixture (Boutonnier 2007; Mahmutovic 2016; Boutonnier et al. 2019). This first step makes it possible to compute an effective modulus and estimate the pore pressure generated during the pressuremeter test when the boundaries move.

A more realistic approach has since been developed, accounting for the non-linearity of the skeleton's response (a G/Gmax law as a function of strain), with strain being maximal near the probe and tending toward zero at infinity (Monnet and Boutonnier 2025).

In the past, several studies have addressed the phenomenon of pore pressure generation (Clarke et al. 1979; Alzubaidi, 2019), but the occurrence of this pore pressure during the pressuremeter test has long been debated. Recently, we demonstrated that the appearance of pore pressure is linked to the non-linear elasticity of the soil (Monnet et al. 2021). For fine soils with a compressible fluid, pore pressure dissipation around the probe results in a 1D radial consolidation process analogous to 1D vertical consolidation in an oedometer. Previous studies mainly approached this phenomenon experimentally (Baguelin et al. 1972), analytically without considering pore pressure (Baguelin et al. 1976), around piles (Niarchos 2012), with only a linear elastic analysis (Clarke et al. 1979) or without distinguishing

between pore pressure and effective stresses (Gibson and Anderson 1961; Hughes and Whittle 2023). The evolution of pore pressure and total stress is not described along the radius.

Consolidation under pressuremeter loading is governed by the pressuremeter consolidation coefficient, c_h (related to the elastic modulus and horizontal permeability k_h), as well as time. It must be addressed by separating the action of the pore water from that of the solid skeleton. This study fully formalizes the mechanism, explicitly defines the effective stress state along the radius, and validates the solution using measurements conducted on Bransley clay (Anderson et al. 1987).

2. Theory – assumptions

The following assumptions are used in this study

2.1. Coordinates

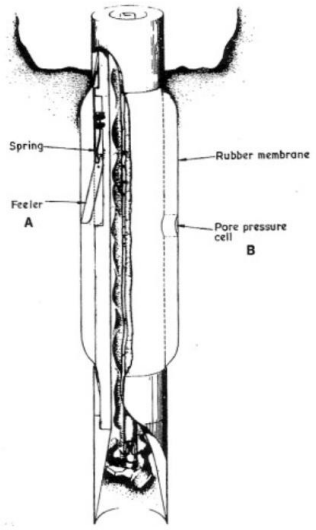

Figure 1: the pressuremeter used (Clarke et al. 1979)

In the case of the pressuremeter (**Fig. 1**), where a total pressure p is applied to the borehole wall at radius a, the pore pressure u_w is measured at the borehole wall. The study is conducted in cylindrical coordinates.

2.2. Mass conservation

We note ε_v the volume variation of the element of soil. $\vec{V}$ is the speed of the interstitial fluid which moves only on the radial direction because V_θ and V_z are null.

$$\frac{\partial \varepsilon_v}{\partial t} = -\frac{1}{r}.\frac{\partial (r.V_r)}{\partial r} = \frac{1}{r}.V_r + \frac{d(V_r)}{dr} \qquad (1)$$

2.3. Darcy Law

The Darcy law is applied, which gives a relation between the water speed V_r and the variation of the pore pressure u_w : with k soil permeability; γ_w the bulk density of the interstitial fluid; u_w the pore pressure

$$V_r = -[k_h/\gamma_w].[\partial u_w/\partial r] \qquad (2)$$

$$\frac{\partial \varepsilon_v}{\partial t} = \frac{1}{r}.\frac{\partial (r.V_r)}{\partial r} = \frac{k_h}{\gamma_w}.\frac{1}{r}.\frac{\partial (r.u_w)}{\partial r} \qquad (3)$$

2.4. Relation between volume variation and pore pressure :

Previous works had shown the interstitial fluid is composed of water and air bubbles even into soil that is commonly considered as saturated (Monnet and Boutonnier 2024). For this compressible fluid, the volume variation is linked to the volume variation by $\mathbf{c_f}$ the compressibility coefficient of the mix water + air; n is the porosity of the soil and assumed constant.

$$\varepsilon_v = -[\mathbf{c_f}.\mathbf{n}.\mathbf{du_w}]/dt \qquad (4)$$

2.5. Terzaghi condition:

The total pressure p is applied on the borehole wall for the radius a; it is considered as a constant and independent of the time. This implies that the total pressure in any radius value is also constant considering time. The Terzaghi relation is used :

$$\boldsymbol{\sigma = \sigma' + u_w = Cte} \qquad (5)$$

$$\partial \sigma'/\partial t = -\partial u_w/\partial t \qquad (6)$$

2.6. Non-saturation condition:

It is assumed that the soil is in D3 state (Boutonnier 2007), i.e partial saturation with a mixture of water and air; this leads to c_h the apparent consolidation coefficient, with c_f the compressibility coefficient of the mix soil + fluid + air

$$c_h = k_h/[\gamma_w.\mathbf{c_f}.\mathbf{n}]. \qquad (7)$$

2.7. Small deformation

To simplify the theory, it is assumed small deformations

2.8. Non-linear elasticity

A non-linear elasticity is assumed Eq. (8) (**Figure 2**) so that the apparition of the pore pressure is possible (Monnet and Boutonnier 2024)

$$\mathbf{G_s}/G_{max} = 1/[1 + 0.385.\gamma/\gamma_{0.7}] \qquad (8)$$

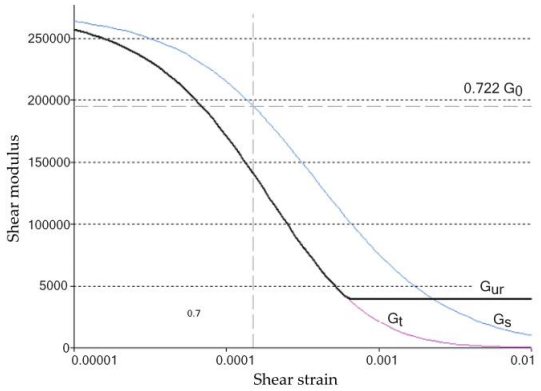

Figure 2: Theory : Evolution of the shear and secant modulus assumed (Plaxis 2012)

3. Constant B_{pres} theory – developments

3.1. Relation between total and effective stress

Following (Skempton 1954) we consider a linear relation Eq. (9) between pore pressure and total pressure, as observed on pressuremeter performed with cycles into clay (**Figure 3**). This linearity implies a linear relation between total and effective stress Eq. (10) with B_{pres} the Skempton coefficient applied to the pressuremeter; G'$_s$ is the secant shear modulus. The right-hand side of Eq. (9) can be derived as follows.

$$\delta u_{wi}/\delta\sigma_r = B_{pres} = 1/\left(1 + c_f.n.G'_s\right) \quad (9)$$

$$\delta\sigma'_r = \delta\sigma_r\left(1 - B_{pres}\right) \quad (10)$$

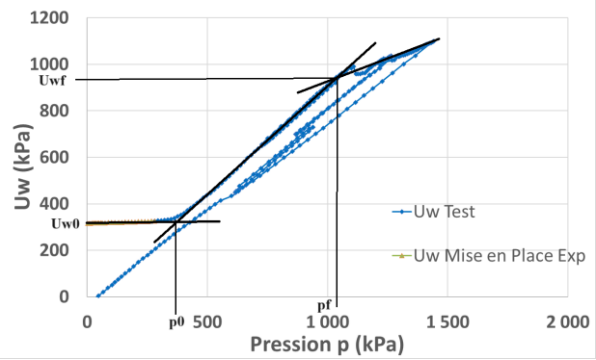

Figure 3: Experience : linear relation between the measured pore pressure and the total pressure – pressuremeter test in London clay at 20,8m depth (Monnet and Boutonnier 2024)

3.1. Equilibrium condition and resolution

The equilibrium condition of the unit volume (**Figure 4**) is governed by the following equations:

$$\sigma_r - \sigma_\theta + r.\frac{d\sigma_r}{dr} = 0 \quad (11)$$

$$\sigma'_r - \sigma'_\theta + r.\frac{d\sigma'_r}{dr} + r.\frac{du_w}{dr} = 0 \quad (12)$$

Eq. (11) gives the equilibrium of the unit volume in total stress but if we consider the pore pressure, it becomes Eq. (12) in effective stress.

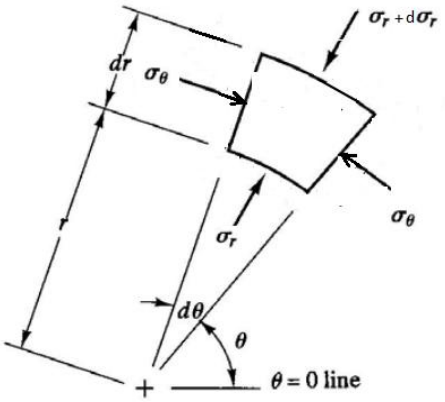

Figure 4: Equilibrium of the unit volume

Shear stress differences can be expressed in terms of total or effective stress:

$$\sigma_r - \sigma_\theta = \sigma_r' - \sigma_\theta' \quad (13)$$

Considering the symetry Eq. (14) between the effective stresses and the initial effective pressure at rest (Monnet and Boutonnier 2024), shearing can be written along (16)

$$\sigma'_r - p_0' = p_0' - \sigma_\theta' \quad (14)$$

$$\sigma'_\theta = 2.p'_0 - \sigma'_r \quad (15)$$

$$\sigma_r - \sigma_\theta = \sigma'_r - \sigma_\theta' = 2.\sigma'_r - 2.p'_0 \quad (16)$$

Using the linear relation between pore pressure and total stresss (Skempton 1954) and the experimental relation (**Figure 3**), Eq. (17) and Eq. (18) are written;.

$$du_w = B_p.d\sigma_r \quad (17)$$

$$u_w = B_{pres}.\left(\sigma_r - p_0\right) + u_{w0}\ pour\ p \geq p_0 \quad (18)$$

using the Terzaghi relation Eq. (5) and the symetry of the effective stress versus p'$_0$ the effective horizontal pressure at rest (Monnet and Boutonnier 2024). The shearing becomes Eq. (19). Introducing Eq. (19) into the equilibrium Eq. (12) we find a First-order differential Eq. (21) which becomes Eq. (22).

$$\sigma_r - \sigma_\theta = \sigma'_r - \sigma_\theta' = \sigma'_r - 2.p'_0 + \sigma'_r = 2.\sigma'_r - 2.p'_0 \quad (19)$$

$$r.\frac{d\sigma_r}{dr} + \sigma'_r + u_w + \sigma'_r - 2.p'_0 - u_w = 0 \quad (20)$$

$$r.\frac{d\sigma_r}{dr} = -(\sigma'_r - \sigma'_\theta) = -2.\left(\sigma'_r - p'_0\right) = -2.\left(\sigma_r - p_0\right)\left(1 - B_{pres}\right) \quad (21)$$

$$-\frac{d\sigma_r}{2.\left(\sigma_r - p_0\right)\left(1 - B_{pres}\right)} = \frac{dr}{r} \quad (22)$$

The solution of Eq. (22) can be found into Eq. (23), which allows to know the distribution of the total stress Eq. (24) and the pore pressure Eq. ((25) and the effective stress Eq. (26) Eq. (27) along the radius

$$\frac{\left(\sigma_r - p_0\right)}{\left(p - p_0\right)} = \left(\frac{a}{r}\right)^{[2.(1-B_p)]} \quad (23)$$

$$\sigma_r = \left(p - p_0\right).\frac{a^{[2.(1-B_p)]}}{r} + p_0 \quad (24)$$

$$u_w. = B_{pres}.\left(\sigma_r - p_O\right) + u_{w0} \quad (25)$$

$$\sigma'_r = \left(1 - B_{pres}\right)\left[\left(p - p_0\right)\left(\frac{a}{r}\right)^{2.(1-B_{pres})}\right] + p'_0 \quad (26)$$

$$\sigma'_\theta = -\left(1 - B_{pres}\right)\left[\left(p - p_0\right)\left(\frac{a}{r}\right)^{2.(1-B_{pres})}\right] + p'_0 \quad (27)$$

Please note that Eq. (23) to Eq. (27) are independent of the shearing modulus.

4. Constant B_{pres} theory – validation

Validation of Eq. (25) can be performed by comparison with the experimental results (Anderson et al. 1987) where the measurement of the pore pressure was carried out at 3 differents values of the radius. For the second test of (Anderson et al. 1987), we found that the pore pressure decrease more than the theoretical relation; as a consequence we assume for the outer values

of the pore pressure a linear variation Eq. (30) of σ_r and u_w between $L_d/2.a$ and $L_d.a$ where the pore pressure return to u_{w0}; L_d is a parameter of the model which rules the extension od the area impacted by the pressuremeter test. The outer linear variation of u_w is ruled by Eq. (28) with the coefficients A_0 and A_1 Eq. (29)..

$$u_{wd} = B_{pres}.\left[(p - p_0)\left(\frac{2}{L_d}\right)^{2.(1-B_{pres})}\right] + u_{w0} \quad (28)$$

$$A_1 = -2.\frac{(u_{wd} - u_{w0})}{L_d.a} \; ; \; A_0 = u_{w0} - A_1.L_d.a \quad (29)$$

$$u_w = A_0 + A_1.R \quad (30)$$

The comparaison between the theoretical pore pressure and the measured one is shown on (**Figure 6**; **Figure 7**), and the parameters used are in (**Table 1**). In this analysis a linear response of the pore pressure is found versus the total pressure applied so that the loading can be considered as undrained below 100kPa (**Figure 5**). All results are documented (Monnet and Boutonnier 2025)

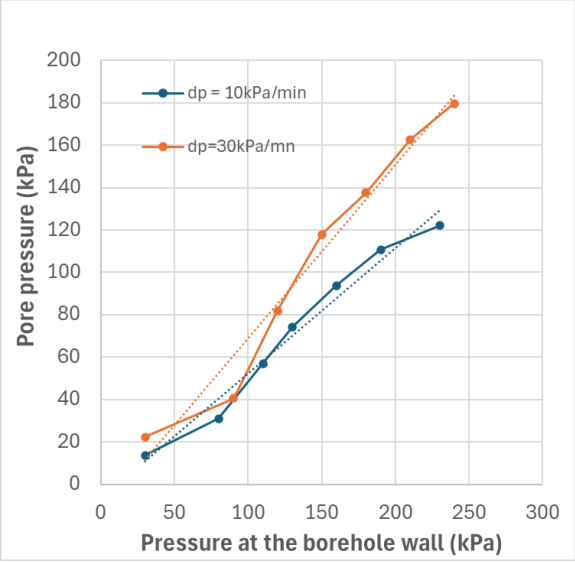

Figure 5: Evolution of the pore pressure at the borehole wall versus the total pressure applied; Two loading speeds (10 and 30kPa/Min.) (Anderson et al. 1987)

Table 1 : Parameters used for the validation of the constant B_{pres} theory on the laboratory test (Anderson et al. 1987)

	Δp=10kPa/min	**Δp=30kPa/min**
u_{w0} (kPa)	0	0
B_p	0.59	0.75
p_0 (kPa)	0	0
L_d	5	5

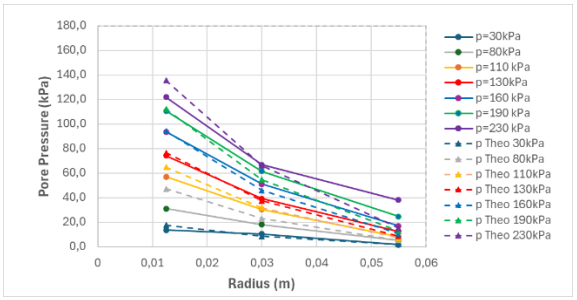

Figure 6: Evolution of the pore pressure along the radius for the test with Δp=10kPa/Min. (Anderson et al. 1987)

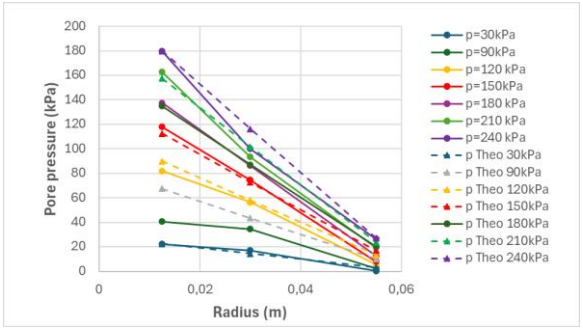

Figure 7: Evolution of the pore pressure along the radius for the test with Δp=30kPa/Min. (Anderson et al. 1987)

5. Consolidation theory – developments

5.1. Consolidation equation

Combining Eq. (*2*) and Eq. (*1*), we find the consolidation Eq. (*31*) which can be rewritten Eq. (33)

$$-\mathbf{c_f}.\mathbf{n}.\frac{\mathbf{du_w}}{\boldsymbol{dt}} = -\frac{\boldsymbol{k_h}}{\boldsymbol{\gamma_w}}.\frac{\mathbf{1}}{\boldsymbol{r}}.\frac{\boldsymbol{\partial(r.u_w)}}{\boldsymbol{\partial r}} \quad (31)$$

$$\frac{\boldsymbol{\gamma_w}.\mathbf{c_f}.\mathbf{n}}{\boldsymbol{k_h}}.\frac{\mathbf{du_w}}{\boldsymbol{dt}} = \frac{\mathbf{1}}{\boldsymbol{r}}.\frac{\boldsymbol{\partial(r.u_w)}}{\boldsymbol{\partial r}} \quad (32)$$

$$\frac{\boldsymbol{\gamma_w}.\mathbf{c_f}.\mathbf{n}}{\boldsymbol{k_h}}.\frac{\boldsymbol{du_w}}{\boldsymbol{dt}} = \frac{\mathbf{1}}{\boldsymbol{C_h}}\frac{\boldsymbol{du_w}}{\boldsymbol{dt}} = \left(\frac{\boldsymbol{d^2u_w}}{\boldsymbol{dr^2}} + \frac{\mathbf{1}}{\boldsymbol{r}}.\frac{\boldsymbol{du_w}}{\boldsymbol{dr}}\right) \quad (33)$$

5.2. Separation of variables

To solve Eq. (*33*), we notice that the left part depends of the time and the right part depends on the radius so the solution can be written as Eq. (*34*), and the two parts of equation Eq. (*33*) must be equal to the same constant value $-\boldsymbol{\lambda^2}$ Eq. (*35*):

$$\boldsymbol{u_w(r,t) = X(r).T(t)} \quad (34)$$

$$\frac{\mathbf{1}}{\boldsymbol{c_h}}\frac{\boldsymbol{du_w}}{\boldsymbol{dt}} = \left(\frac{\boldsymbol{d^2u_w}}{\boldsymbol{dr^2}} + \frac{\mathbf{1}}{\boldsymbol{r}}.\frac{\boldsymbol{du_w}}{\boldsymbol{dr}}\right) = -\boldsymbol{\lambda^2} \quad (35)$$

5.3. Solution depending on time:

The time part of Eq. (*35*) is now Eq. (*36*) and can be solved by Eq. (*37*). The condition of T(t)=1 for t=0 gives T_0=1.

$$\frac{\mathbf{1}}{\boldsymbol{T(t)}}.\frac{\boldsymbol{\partial T(t)}}{\boldsymbol{\partial t}} = -\boldsymbol{\lambda^2}.\boldsymbol{c_h} \quad (36)$$

$$\boldsymbol{T(t) = T_0.exp^{-\lambda_n^2.c_h.t} = exp^{-\lambda_n^2.c_h.t}} \quad (37)$$

5.4. Solution depending on radius:

The spatial part of Eq. (*35*) is now Eq. (*38*) and can transformed multiplying X(r) into Eq. (*39*). Changing the variable into Eq. (*40*) the equation is rewrite into Eq. (*41*). This latest form is the Bessel equation of order zero. It solution is known as Eq. (*42*) with the Bessel functions of first order J_0 and Y_0, and the constants A and B.

$$\left(\frac{1}{X(r)}\frac{\partial^2 X(r)}{\partial r^2}+\frac{1}{r.X(r)}.\frac{\partial X(r)}{\partial r}\right)=-\lambda^2 \quad (38)$$

$$\frac{\partial^2 X(r)}{\partial r^2}+\frac{1}{r}.\frac{\partial X(r)}{\partial r}+\lambda^2.X(r)=0 \quad (39)$$

$$X(r)=Z(r)/r \;\; ; \;\; and \;\; \rho=r.\lambda \quad (40)$$

$$\frac{\partial^2 Z(\rho)}{\partial \rho^2}+\frac{1}{\rho}.\frac{\partial Z(\rho)}{\partial \rho}+Z(\rho)=0 \quad (41)$$

$$X(\rho)=A.J_0(\rho)+B.Y_0(\rho) \quad (42)$$

5.5. Condition on radius – null increase of pore pressure after L_d.a

At a distance of L_d.a the increase of pore pressure given by the pressuremeter is null. This condition gives the Eq. (*43*), with the variable Eq. (*44*). But Eq. (*42*) can be rewritten as Eq. (*45*) with the new inner constant α Eq. (*46*) which depends on $J_0(\rho_d)$ and $Y_0(\rho_d)$. The inner coefficient α is now known Eq. (*46*) through the known values of $J_0(\rho_d)$ and $Y_0(\rho_d)$.

$$X(L_d.a)=0 \quad (43)$$

$$\rho_d=\lambda\;.L_d.a\;=L_d.\rho_a \quad (44)$$

$$X(L_d.a)=A.[J_0(\rho_d)+\alpha.Y_0(\rho_d)]=0 \quad (45)$$

$$\alpha=-\frac{J_0(\rho_d)}{Y_0(\rho_d)}=\frac{B}{A} \quad (46)$$

5.6. Condition on radius – imposed increase of pore pressure at radius a for t=0

This condition impose $X(a)=u_{wi}$ which give Eq. (*47*) and the value of A Eq. (*48*):

$$X(a)=A.J_0(\rho_a)+A.\alpha.Y_0(\rho_a)=u_{wi} \quad (47)$$

$$A=\frac{u_{wi}}{J_0(\rho_a)+\alpha.Y_0(\rho_a)} \quad (48)$$

5.7. General solution of consolidation:

The general solution of consolidation is now:

$$u_w(r,t)=A.[J_0(\rho)+\alpha.Y_0(\rho)].exp^{-\lambda^2.c_h.t} \quad (49)$$

6. Consolidation theory – validation

6.1. Measurement of linear relation between the decrease of pore pressure and the time:

At a given value of the radius, for instance r=a, the consolidation theory shows an exponential relation between the increase of pore pressure and the time of slope $-\lambda^2.c_h$ Eq. (*37*). This theoretical results is retrieved experimentally by the linear relation between the logarithm of the excess of pore pressure versus the time (**Figure 8**). It appears that the mean slope is constant for pressure lower than 100kPa and increase when p is higher. We interpret this evolution by the effect of a plastic behaviour which is not in the frame of our study. The mean value of the slope is shown in (**Table 2**). The other parameters are in (**Table 1**).

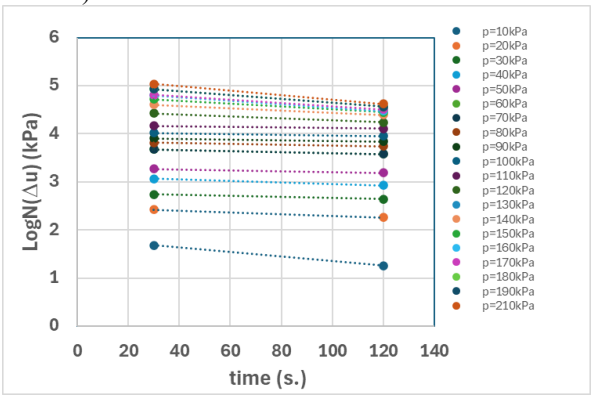

Figure 8: Evolution of the increase of pore pressure along time for different values of loading

6.2. Evolution of the pore pressure along the radius:

For the Bransley clay specimen the evolution of the pore pressure along the radius is measured after 1min. (Anderson et al. 1987) and can be compared (**Figure 9**) with the results issued from the constant B_{pres} theory, and the results issued from the consolidation theory with 4 different times of consolidation. It can be observed that either the Constant B_{pres} theory and the Consolidation theory fit quite well with the experimental results, but the consolidation theory presents an evolution more smoothy with no break point. Furthermore, it allows finding the pore pressure at different level of time.

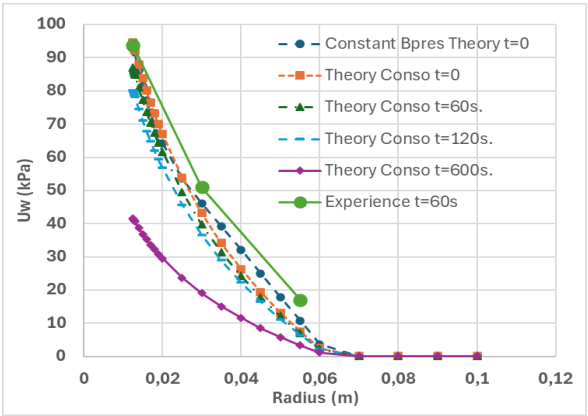

Figure 9: Evolution of the pore pressure along the radius for the test with Δp=30kPa/Min.

6.3. Evolution of the pore pressure along the time:

For the Bransley clay specimen (Anderson et al. 1987) the evolution of the pore pressure along the radius is measured 15s. after the loading and with an holding time of 60s. (**Figure 10**) or 120s. (**Figure 11**) and can be compared with the theoretical results issued from the consolidation theory. On (**Figure 10**) and (**Figure 11**) experimental results are in solid line while theoretical

Table 2 : Parameters used for the validation of the consolidation theory on the laboratory test (Anderson et al. 1987)

	Δp=10kPa/min	Δp=30kPa/min
Slope (kPa/s)	0.0137	------

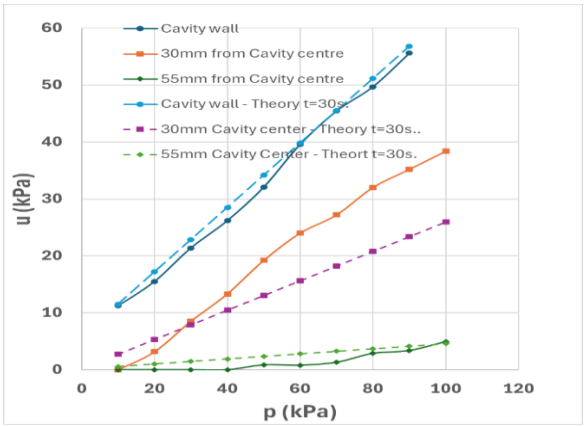

Figure 10: Evolution of the pore pressure along the radius for the test with Δp=10kPa 15s. after loading 30s., holding time

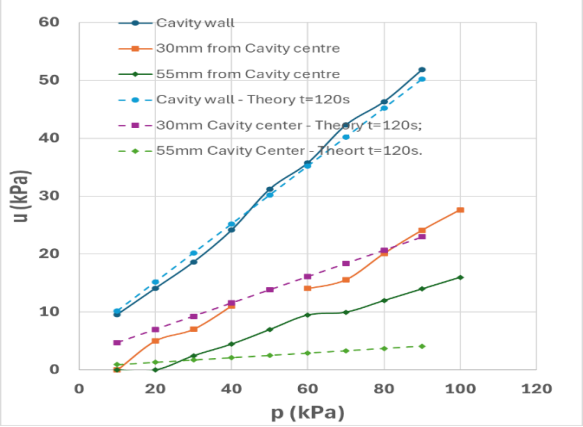

Figure 11: Evolution of the pore pressure along the radius for the test with Δp=10kPa 15s. after loading, 120s. holding time

ones are in dotted line. The evolution of the pore pressure is captured at the cavity wall for the two experiences, while the measurement at 30mm from the center is higher than the theoretical result at 60s of holding time, and the measurement at 55mm is also higher than the theory at 120s. of holding time. But it appears that the main evolution of the pore pressure is retrieved by the theory.

The parameters used are shown (**Table 2**), and the other parameters are in (**Table 1**).

7. Conclusion

In this study, we proposed two complementary approaches to analyze the evolution of pore pressure around the pressuremeter at varying distances from the borehole wall. The first approach is based on a constant B_{pres} coefficient and assumes equilibrium of effective stresses; it provides a global distribution of pore pressure during loading. The second approach incorporates water flow governed by Darcy's law, effective stress equilibrium, and the non-linear elastic behavior of the soil; it enables accurate reproduction of experimental pore pressure values at different radial distances and consolidation times, which is not possible with previous models. At this stage of development, an additional condition is needed to determine the constant λ, so that the experimentally measured slope $\lambda^2 c_h$ can be used to identify the horizontal consolidation coefficient c_h.

8. References

Alzubaidi, R., 2019. Effect rate of strain on in situ horizontal coefficient of consolidationfrompressuremeter. Geotech. Geol. Eng. 38, 1669–1674. https://doi.org/10.1007/s10706-019-01122-6 (0123456789().,-volV

Anderson, W.F., Pyrah, I.C., Ali Faisal, H., 1987. Rate effects in Pressuremeter tests in clays. J. Geotech. Eng. ASCE 113, 1344–1358.

Baguelin, F., Jezequel, J.F., Le Mee, E., Le Mehauté, A., 1972. Expansion de sondes cylindriques dans les sols cohérents. Bull Liaison Labo P C H.

Baguelin, F., Jezequel, J.F., Le Mehauté, A., 1976. Mesure des caractérstiques des sols par autoforage. Bull Liaison Labo P C H 81, 63–72.

Boutonnier, L., 2007. Comportement hydromécanique des sols fins proches de la saturation. Cas des ouvrages en terre : coefficient B, déformations instantanées et différées, retrait / gonflement. Thèse INPG Grenoble.

Boutonnier, L., Bufalo, M., Dubreucq, T., Fry, J.-J., Lejeune, J.-M., Mahmutovic, D., 2019. Conception et construction des ouvrages en sol fins - Enseignements du projet ANR Terredurable et retour d'expérience, Presses des Ponts. Presses de l'ENPC/LCPC, Paris.

Clarke, B.G., Carter, J., Wroth, C.P., 1979. In situ determination of the consolidation characteristics of saturated clays, in: 7th European Conference on Soil Mechanics and Foundation engineeringAt: Brighton. Brighton, pp. 207–211.

Gibson, R.E., Anderson, W.F., 1961. In-Situ measurement of Soil Properties with the pressuremeter. Civ. Rng Public Works Rev. 615–618.

Hughes, J., Whittle, R.W., 2023. High resolution pressuremeters - the measurement of small things. CRC Press - Taylor & Francis Group, Boca Raton.

Mahmutovic, D., 2016. Etude du comportement des sols proches de la saturation – validation numérique sur essais de laboratoire et ouvrages en terre. Université de Grenoble Alpes, Grenoble.

Monnet, J., Boutonnier, L., Mahmutovic, D., 2021. Elastic interpretation of unsaturated undrained pressuremeter tests in clays, in: 6th International Conference on Site Characerisation. Budapest, pp. 1–6.

Monnet, J., Boutonnier, L., 2024. Interpretation of the pressuremeter test into clay in unsaturated and undrained condition, in: 7th Int. Conf. on Geot. and Geophys. Site Characterisation. Barcelonne, pp. 1–8.

Monnet, J., Boutonnier, L., 2025. Interprétation du pressiomètre en Non-Drainé Non-Saturé – application a l'argile de Londres. Rev. Francaise Geotech.to be published.

Niarchos, D.G., 2012. Analysis of consolidation around driven piles in overconsolidated clay (PhD Thesis). Massachussetts Institute of Technology.

Plaxis, 2012. Plaxis 2D - Reference manual.

Skempton, A.W., 1954. The Pore-Pressure Coefficients A and B | Géotechnique. Géotechnique 4, 143–147.